Wear 462-463 (2020) 203490

Contents lists available at ScienceDirect

Wear

journal homepage: http://www.elsevier.com/locate/wear

Influence of laser shock peening on the surface energy and tribocorrosion properties of an AZ31B Mg alloy

Arpith Siddaiah, Ph.D., Bo Mao, Ph.D., Ashish K. Kasar, Yiliang Liao, Ph.D. **, Pradeep L. Menezes, Ph.D. *

Department of Mechanical Engineering, University of Nevada, Reno, Reno, NV 89557, USA

ARTICLE INFO

Keywords:
Wear-corrosion synergism
Laser shock peening
Surface roughness
Interfacial surface energy

ABSTRACT

The present study investigates the influence of laser shock peening (LSP) on surface energy (S_E) of AZ31B Magnesium alloy and its resilience to corrosion and tribocorrosion. AZ31B alloy was treated at different laser intensities. The S_E and its interfacial components of treated surfaces were analyzed. The S_E was found to be least at low laser intensity LSP. Lower interfacial S_E showed decreased wettability, providing enhanced tribocorrosion resistance with respect to untreated surface. However, higher laser intensities increased the surface roughening effect, causing an increase in the interfacial S_E and wettability of the surfaces, decreasing the tribocorrosion resistance. The study finds LSP can enhance tribological properties and mitigate the effects of corrosion and tribocorrosion.

1. Introduction

Magnesium (Mg) alloy, specifically AZ31B, is an exceptionally ductile material that is 35% lighter than aluminum with high machinability [1–4], which enables easy surface modifications [5–9]. Even though AZ31B has broad applicability as lightweight structural and mechanical parts for medical, aerospace, and automobile applications [10–15], it still has poor corrosion resistance and needs to be anodized to improve its durability for mechanochemical applications [16–19]. AZ31B has significant potential as biomedical implants due to its excellent biocompatibility as well as adequate mechanical properties [13,20,21]. However, the biocompatibility of this alloy is only significant if it can provide considerable wear and corrosion resistance [17]. Generally, the surface properties of AZ31B are optimized by laser or mechanical treatments while fabricating the alloy.

Considering the potential of Mg alloy, it is necessary to understand how the surface processing and surface modification techniques affect not just the wear and corrosion properties but also the tribocorrosion properties (wear-corrosion synergism). Wear-corrosion synergism results from the interaction of wear and corrosion in an aqueous environment, which leads to a faster materials degradation rate as compared to wear or corrosion occurring separately. This degradation process is referred to as tribocorrosion. Recent studies on the tribological and tribocorrosive effects of laser shock peening (LSP) and other such surface engineering processes have provided significant insight into the role of surface roughness, hardness, and residual stresses in defining the wear, corrosion, and tribocorrosion mechanisms [5,6,22]. The application of AZ31B can be sustainable only if the tribological and tribocorrosive mechanisms are understood in various aqueous environments. In environments susceptible to corrosion, the surface roughness (SR) can drastically modify the wettability of the surface by affecting the surface energy (S_E). The change in SR is more drastic in the case of Mg alloys due to their high ductility [6,22–24]. The change in S_E and wettability alters how aqueous solutions interact with the surface, and thus results in altered wear, corrosion, and tribocorrosion behavior.

The work required in order to hold a unit surface area intact is defined as S_E in solids and liquids. In liquids, the mobility of the molecules enables them to easily attain equilibrium. Whereas in a solid the molecules are not mobile enough to minimize the surface area and achieve equilibrium. The S_E is a key parameter to define the wettability of the surface with a liquid of known surface tension. Even though it is possible to measure of wetting in terms of contact angle, it does not provide qualitative and quantitative information of the interfacial forces between the solid and liquid, the solid and vapor, and the liquid and

* Corresponding author.
** Corresponding author.
E-mail addresses: asiddaiah@nevada.unr.edu (A. Siddaiah), bmao@nevada.unr.edu (B. Mao), akasar@nevada.unr.edu (A.K. Kasar), yliao@unr.edu (Y. Liao), pmenezes@unr.edu (P.L. Menezes).

https://doi.org/10.1016/j.wear.2020.203490
Received 20 April 2020; Received in revised form 23 August 2020; Accepted 15 September 2020
Available online 25 September 2020

vapor interfaces. This makes it difficult to quantify the S_E of the solids, especially when influenced by SR. Currently, the most effective method to calculate S_E is the approach based on Lewis acid-base surface interaction components. The three-component approach was developed by Van Oss et al. [25,26] which can adequately separate the S_E components and determine the interfacial S_E as the indicator for solubility. It was shown that in polar systems the S_E involves Lifshitz-van der Waals (LW) and polar acid-base (AB) interactions:

$$\gamma_s^{tot} = \gamma_s^{LW} + \gamma_s^{AB}$$

where γ_s^{tot} is the total S_E of the solid (s). The acid-base component of S_E is given by the geometric mean of γ_s^{AB+}, electron acceptor, and γ_s^{AB-}, electron donor given by:

$$\gamma_s^{AB} = 2\sqrt{\gamma_s^{AB-}\gamma_s^{AB+}}$$

The van Oss theory discussed above focusses on separating the surface energy of a solid into three main components as dispersive (LW), acid (AB^+), and base (AB^-) components. The dispersive component will characterize the non-specific interactions such as van der Waals interactions of the solid surface with the liquid while the acid-base components dictate the polar nature of the surface. The acid component characterizes the propensity of a surface to interact via dipole-dipole, induced dipole-dipole, and hydrogen bonding. The base component characterizes the propensity of the solid surface to interact with a liquid having affinity of electrons. The interfacial energy between the solid (s) and liquid (l), γ_{sl}, can be expressed as:

$$\gamma_{sl} = \gamma_s + \gamma_l - W_a$$

where W_a is work due to adhesion that defines the work necessary to pull apart two surfaces in contact and γ_l is the liquid surface tension. Using the above equations, W_a is:

$$W_a = 2\left(\sqrt{\gamma_s^{LW}\gamma_l^{LW}} + \sqrt{\gamma_s^{AB-}\gamma_l^{AB+}} + \sqrt{\gamma_l^{AB-}\gamma_s^{AB+}}\right)$$

Considering the experimentally determined contact angle with probe liquid (θ) with γ_l of the probe liquid and γ_{sl} we get the Young equation for determining S_E of the solid as:

$$\gamma_s = \gamma_l \cos\theta + \gamma_{sl}$$

Studies have shown that the surface energy of Mg alloys can vary drastically based on the basal plane orientation on the surface interacting with liquids. It has been shown that Mg alloys with high basal plane textures exhibit better corrosion resistance compared to those with high prismatic planes on the surface [27]. Experiments have also shown that an increase in surface roughness increases the contact angle of liquid that in turn decreases corrosion on the solid surface [28]. Self-cleaning materials have also been used to address these issues as they minimize water contact angle and therefore, can potentially minimize crucial environmental degradation processes such as corrosion, scaling, biofouling, and accumulation of dirt on the components. Such studies have highlighted the need for investigating the interdependency of surface energy and corrosion behaviors along with their tribological properties.

Surface functionalization using laser-based techniques such as LSP has been studied to modify various properties such as surface hardness [29–32], wear and corrosion resistance [30,33–35], SR [6,36–39], and wettability [40,41]. Tailoring surfaces to have multiple functionalities requires experimental techniques to determine and optimize the process parameters based on the application [5,42–45]. However, without understanding the interactions between surface functionalization's via LSP, it is not possible to understand the full potential of LSP. The present study investigates the influence of LSP on the S_E interactions at the interface of the AZ31B surface and three probe liquids (corrosive and non-corrosive). The study furthers the understanding of surface functionalization using LSP by providing insight into the influence of S_E on corrosion and tribocorrosion properties. The knowledge of S_E changes due to LSP will allow better design AZ31B surface properties for sustainable and diverse applications, including applications in aqueous environments.

Table 1
AZ31B Mg surface nomenclature and their respective laser intensity treatments.

LSP - sample number	Intensity (GW/cm^2)
0 (Untreated)	0
1	0.47
2	0.87
3	1.36
4	1.76
5	2.22

2. Materials and methods

An experimental procedure was developed to study the S_E change due to tribocorrosion on LSP processed AZ31B. The AZ31B block (Al - 3.0 wt%, Zn - 1.0 wt%, and 96 wt% Mg) were cut into six 25 × 25 × 12.5 mm^3 samples for the study. A mean SR value (S_a) of 0.3 ± 0.08 μm was achieved by polishing the samples. The polishing involved grinding the surfaces using sandpapers ranging from 320 to 1200 grit size. Further, a diamond suspension (3 μm) was used to polish the samples to achieve the desired roughness. Among the six polished samples, five surfaces underwent LSP at varying laser intensities and one surface was untreated. The SR, hardness, and contact angle measurements were made on each sample, followed by tribocorrosion testing. The experimental methodology is detailed below.

2.1. LSP of AZ31B surfaces

The laser treatment of the AZ31B surfaces was carried out with a Q-switched Nd-YAG laser (λ = 1064 nm, pulse = 7 ns, beam size = 2.5 × 10^{-3} m). The confinement layer was a BK7 glass which was layered with a black tape ablative coating of thickness of 130 μm [6]. The laser intensity used to process a surface area of 17 × 7 mm^2 is detailed in Table 1, along with the respective nomenclature.

The AZ31B surfaces were LSP processed, as illustrated in Fig. 1a. Fig. 1b shows a 17 × 7 mm^2 surface area that was processed on each sample. The influence of LSP on the S_E and tribocorrosion performance were analyzed by exposing the laser treated area.

2.2. SR and hardness

A Wilson Hardness tester was used to assess the change in hardness due to LSP processing. A load of 500 g was applied with dwell time of 10 s. The variation in SR due to LSP and tribocorrosion on AZ31B surface was analyzed by a 3D optical profilometer. Each surface roughness parameter and hardness measurement were repeated three times. The average of the parameter values is reported with error bars. The error bars for the reported roughness parameter and hardness values were obtained from the standard deviation considering a 90% confidence interval.

2.3. Contact angle and S_E measurements

The total S_E and the solid-liquid interfacial S_E between the LSP processed AZ31B surface and three probe liquids were evaluated using rame-hart contact angle goniometer. Table 2 details the probe liquids used in the study in addition to their total surface tension and surface tension components. A sessile drop method was used to measure the contact angle according to ASTM D7334 - 08 (2013) standards for each LSP processed surface. The study uses a 3-component approach based on

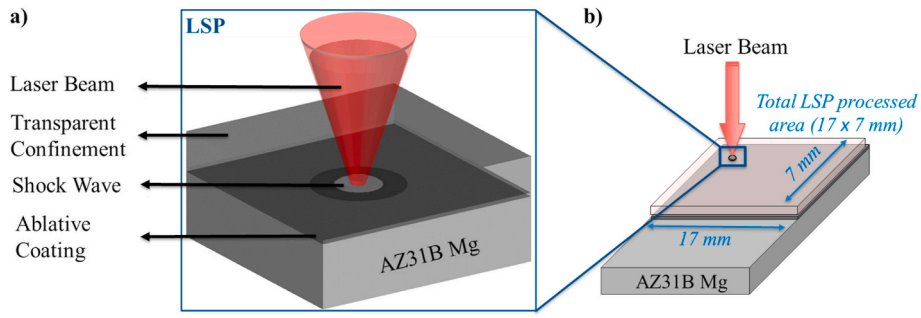

Fig. 1. Illustration of (a) LSP process and (b) LSP processed area on AZ31B surface.

Table 2
Surface tension and its components.

Probe liquid	Total surface tension, γ_l	Dispersive and Lifshitz der Waals component, γ_l^{LW}	Positive polar acid-base component, γ_l^{AB+}	Negative polar acid-base component, γ_l^{AB-}	**Viscosity @24 °C (mPa s)**
Water (W)	72.8	21.8	25.5	25.5	1.01
Glycerol (G)	64	34	57.4	3.92	1069
0.6 M NaCl (N)	73.8	22.2	22	29.6	0.92

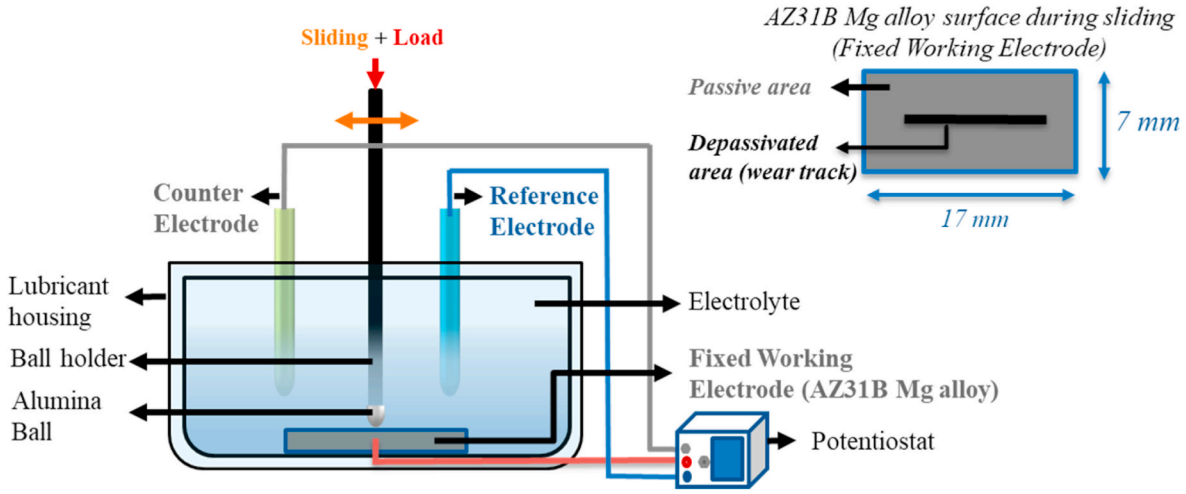

Fig. 2. Representation of tribocorrosion test, and the worn - unworn region on the AZ31B surface during sliding.

Lewis acid-base surface interaction components. The probe liquids, specifically water and 0.6 M NaCl, simulate some of the atmospheric conditions that lead to corrosion on the real surface area exposed to the environment. Sessile drop technique was performed at 24 °C and 20% RH. The probe liquids were collected in a 2 ml syringe to dispense droplet diameters of 2.5–3 mm (6 μl) on the sample surfaces. The contact angle of the droplet for each surface are reported by averaging the observed values over ten trials. The difference in the left and right contact angle of each droplet was less than or equal to 2°. These steps ensured the repeatability and reliability of the contact angle measurements. The interfacial S_E with each probe liquid is determined using the Van Oss [25,26] and Young's equation [46].

2.4. Tribocorrosion tests

The tribocorrosion test set-up involved a combination of reciprocating wear testing and a three-electrode electrochemical test configuration as shown in Fig. 2 [22]. The cell is made up of AZ31B surface - working electrode and a graphite electrode was used as a counter electrode. Whereas, a standard calomel electrode (SCE) was employed as the reference electrode. The equilibrium potential of the open circuit (OCP) was measured for each sample in 3.5% NaCl solution under static conditions. The SCE used in the study has a potential of 0.241 V vs. SHE (standard hydrogen electrode). The reciprocating test on the AZ31B surface was conducted at a speed of 1 mm/s for a total distance of 4000 mm and vertical load of 20 N. The counter material for the reciprocating test was alumina ball of 6.35 mm diameter.

The tribocorrosion test procedure consisted of two stages. The first set of experiments was performed to determine the wear without corrosion by applying cathodic polarization to the AZ31B surface at 1 V below the observed OCP and sliding in 0.6 M (3.5% NaCl solution). The second set of experimentation involved monitoring the OCP of the samples under dynamic conditions to determine the wear-corrosion synergistic effect by sliding with corrosion in 3.5% NaCl solution. Cumulatively, the tribocorrosion test procedure provided the wear-corrosion synergistic effect on wear.

The present study uses the corrosive conditions described in ASTM B895-99, where 0.6 M NaCl is used as the electrolyte. The temperature and humidity conditions during the test were 24 °C and 20% RH, respectively. The test involved in-situ measurement of wear, friction,

Table 3
Surface roughness measurements of LSP processed before and after tribocorrosion testing compared against their LSP processed condition.

Test condition	Surface roughness (μm)				Change in surface area
	S_a	S_p	S_v	S_z	
Untreated	0.3 ± 0.08	0.32 ± 0.06	0.18 ± 0.04	0.74 ± 0.01	0%
After tribocorrosion	3.2 ± 0.18	1.7 ± 0.5	6.0 ± 0.12	7.8 ± 0.4	31.9%
LSP-1	0.35 ± 0.02	0.3 ± 0.03	0.19 ± 0.04	0.92 ± 0.1	1.9%
After tribocorrosion	1.36 ± 0.1	0.8 ± 0.4	1.8 ± 0.5	1.8 ± 0.4	9.0%
LSP-2	0.45 ± 0.02	0.33 ± 0.16	0.2 ± 0.02	1.2 ± 0.2	2.34%
After tribocorrosion	1.7 ± 0.15	1.2 ± 0.1	2.0 ± 0.05	3.3 ± 0.06	23.4%
LSP-3	0.5 ± 0.05	0.65 ± 0.2	0.41 ± 0.06	1.5 ± 0.4	3.1%
After tribocorrosion	2.21 ± 0.13	1.6 ± 0.15	3.33 ± 0.5	4.9 ± 0.7	30.5%
LSP-4	0.6 ± 0.05	0.8 ± 0.1	0.4 ± 0.1	2.2 ± 0.08	6.8%
After tribocorrosion	2.7 ± 0.8	1.4 ± 0.5	1.3 ± 0.4	2.8 ± 0.1	27.8%
LSP-5	0.9 ± 0.06	0.8 ± 0.07	0.9 ± 0.12	2.8 ± 0.05	10.1%
After tribocorrosion	1.5 ± 0.1	1.08 ± 0.09	1.3 ± 0.2	2.4 ± 0.08	24.45%

surface potential, and current variation in the cell. The wear and friction data were collected through reciprocating test while the electrochemical cell was monitored using a potentiostat. Each test was repeated three times for the reproducibility of results. The reported wear behavior in the present study involves understanding the wear-corrosion effects on LSP processed AZ31B surface. The AZ31B surfaces (VHV 62 to 72) are relatively soft as compared to the chemically inert alumina, a ceramic counter body (VHV 1400 to1500). Moreover, due to the LSP on AZ31B, it is expected that subsurface material structural evolution may occur during tribocorrosion and corrosion testing, causing a change in hardness. Hence to accurately interpret the wear loss due to tribocorrosion, the wear tracks for with and without corrosion conditions on AZ31B surfaces were profiled using a 3D optical profilometer. The profiles yielded an accurate estimate of the wear volume for each trail; the average value of wear volume is plotted in Fig. 4 with standard deviation.

The expected worn and unworn regions on the working electrode (sample surface) during sliding is shown in Fig. 2. Following the tribocorrosion tests, the roughness of the exposed surface area was measured [22]. In addition to the SR, the wear track profiles due to sliding in tribocorrosive conditions were also recorded using the profilometer to calculate the wear.

3. Results and discussion

3.1. Influence of LSP on SR

The variation in SR due to LSP on AZ31B surface was analyzed using a 3D optical profilometer. The SR of AZ31B was recorded after polishing the samples to the same mean roughness (S_a) of 0.3 ± 0.08 μm and after LSP at five laser intensities (Table- 1). All measurements were compared against the untreated surface condition of AZ31B (LSP-0, Untreated). The SR of the counter material – alumina ball-was found to have an average SR of 0.01 μm. After the tribocorrosion test, the ball was found to undergo a negligible change in SR as it remained 0.01 μm after completion of LSP and tribocorrosion tests. Additionally, the alumina material being chemically inert and high wear-resistant in such environments, especially when considering the AZ31B as the sliding surface. Thus, the overall surface energy of the AZ31B surface was not expected to affect during the tribocorrosion tests due to the counter alumina material. The observed values of SR parameters for the LSP surfaces were - mean roughness (S_a), maximum peak height (S_p), maximum valley depth (S_v), maximum height (S_z), and change in surface area after LSP are reported in Table 3. These roughness parameters were chosen mainly due to their proven ability to help in perceiving the effect of LSP and tribocorrosion on surface roughness. The S_a parameter is the extension of R_a (arithmetical mean height of a 2D profile line) to a surface. It is expressed, as an absolute value, the difference in height of each point compared to the arithmetical mean of the surface. The S_p is the height of the highest asperity peak, S_v is the absolute value of the height of the largest pit within the defined area, and S_z is defined as the sum of the largest asperity peak height value and the largest pit depth value within the defined area [47].

The plot comparing the change in SR parameters and surface area of LSP processed AZ31B surfaces is shown in Fig. 3. The laser intensities

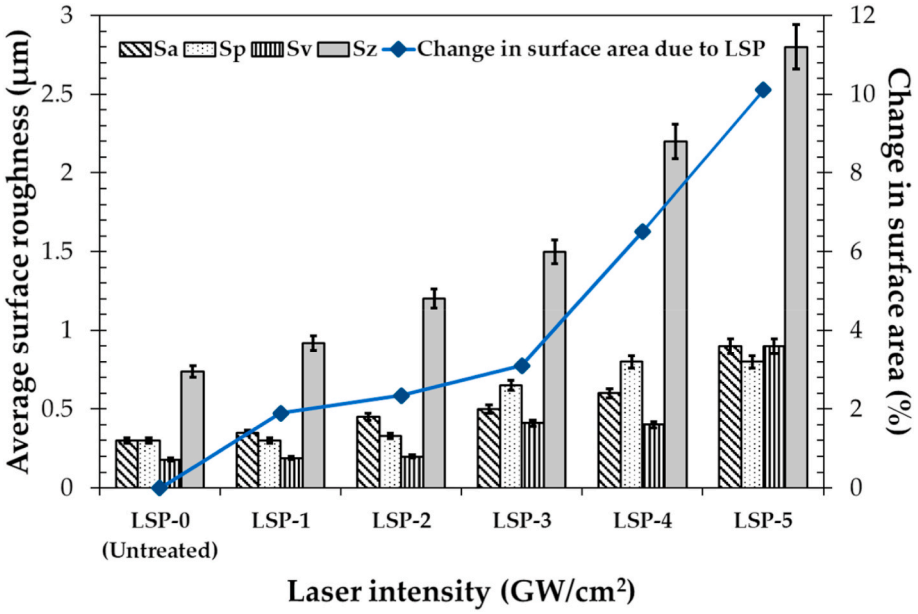

Fig. 3. Surface roughness and area of LSP processed AZ31B alloy.

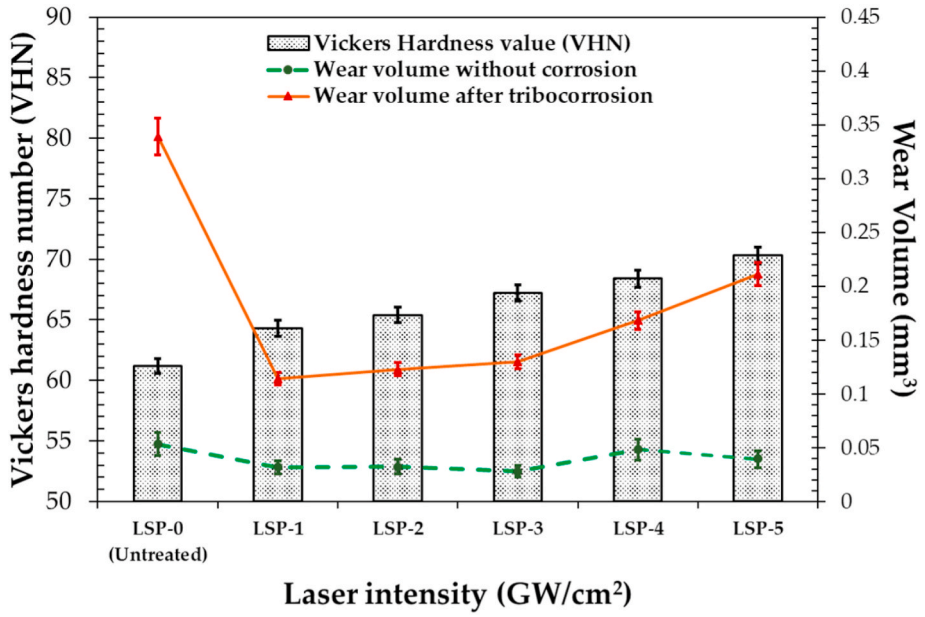

Fig. 4. Wear volume observed on LSP processed surfaces without the influence of corrosion, and after tribocorrosion.

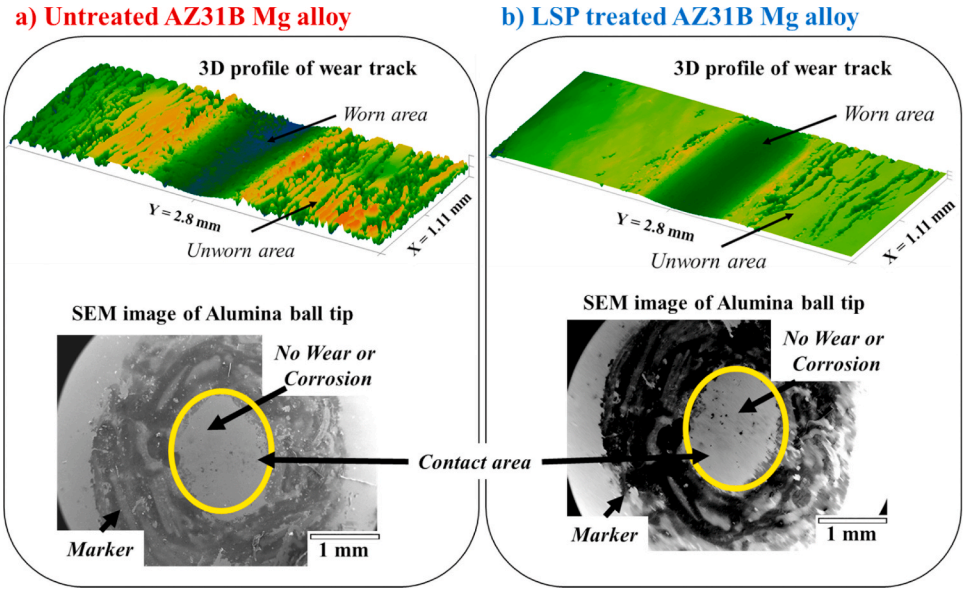

Fig. 5. The presence of wear and corrosion on wear track and its absence on alumina ball tip after tribocorrosion as observed for a) Untreated b) LSP treated AZ31B Mg alloy.

used for LSP were found to have a linear effect on the SR parameters where the SR is increases with laser intensity. This is due to the dimple effect (indents) generated by LSP on the surface, which modifies the surface morphology of the processed area [48]. During LSP, laser shock waves are generated, which induce residual stresses, increase the surface hardness, and generate a variation in the asperity peak heights and valley depths relative to the applied laser intensity. The increased variation in the asperity with laser intensity causes an increase the real surface area that may lead to increased susceptibility of the surface to corrosion. But, it has been shown that the observed change in surface area occurs after LSP is a combination of surface roughening and hardening effects [5,6], which can vary the corrosion inhibition properties of the surface [22,49].

Further, the results show that the change in SR after LSP can be best perceived using S_a, S_p, S_v, and S_z roughness parameters. The LSP is found to have a linear effect on the surface area, which necessitates the study of S_E, especially when considering the application of AZ31B alloy in aqueous environments susceptible to both wear and corrosion.

3.2. Influence of LSP on wear during corrosion

The influence of LSP on tribocorrosion was experimentally studied in terms of wear volume as shown in Fig. 4. The wear after tribocorrosion on LSP processed AZ31B surfaces is observed to be drastic as compared to wear with no corrosion. The maximum wear volume is observed for the untreated surface whereas LSP-1 surface yields least wear volume after tribocorrosion. The untreated surface experienced nearly three times more wear due to tribocorrosion than LSP-1 surface. Also, the observed increase in hardness with laser intensity (LSP-1 to LSP-2) does translate into increased wear resistance, as shown by many studies [6,

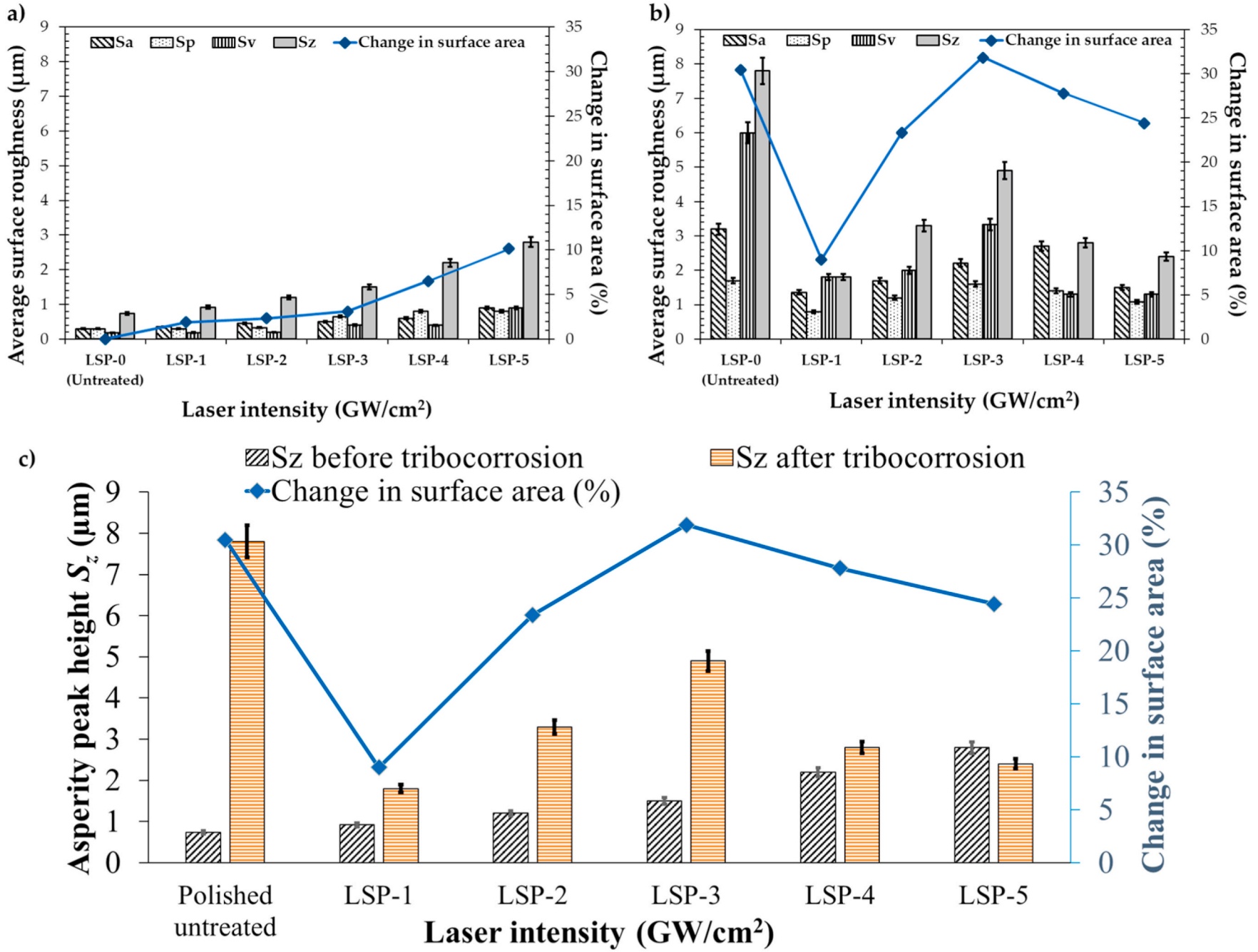

Fig. 6. Surface roughness and area of (a) LSP processed AZ31B,(b) LSP processed AZ31B after tribocorrosion testing, and (c) an S_z specific comparative plot to show the change in asperity height due to tribocorrosion.

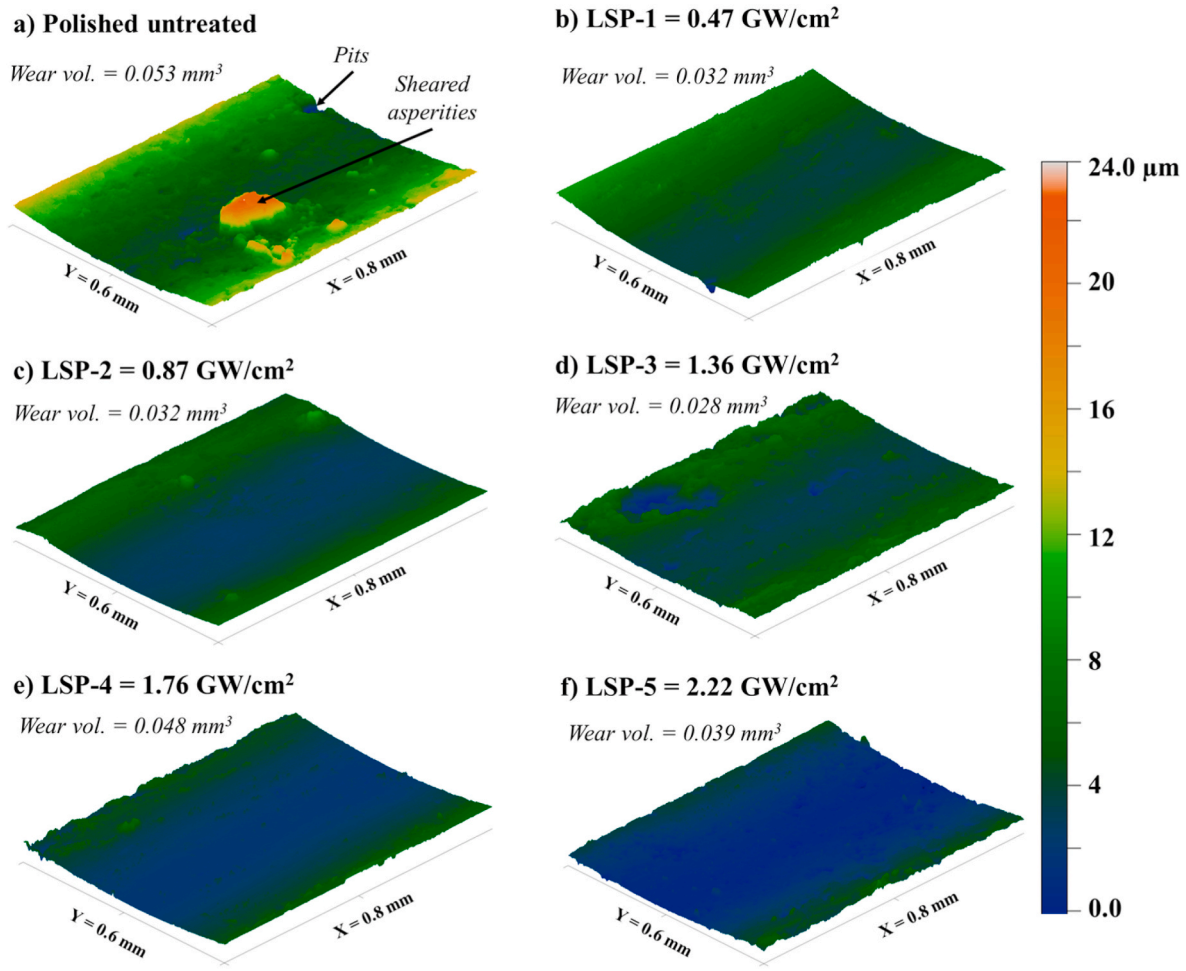

Fig. 7. Wear track profiles after reciprocating tests without corrosion on AZ31B surfaces processed at various laser intensities (a–f).

29–32,36–39]. The hardness of the AZ31B surface (VHV 62 to 72) is ~23 times less than the hardness of the counter body, alumina ball (VHV 1400 to 1500). Considering this large difference in hardness between the surface and the counter body, the plowing effect of the counter body should lead to abrasive wear on the surface during sliding. Additionally, alumina being a ceramic material, has been well studied to be electrochemically inert with high wear resistance [50,51].

The presence of wear and corrosion products on the ball was verified under an SEM, as shown in Fig. 5. The figure shows that the effects of tribocorrosion on AZ31B surface and alumina ball for untreated and LSP treated conditions. The reaction products are fairly evident on the ball tip in Fig. 5. The particles adhered to the ball indicate the presence of a sub mechanism that participates in the wear and corrosion during tribocorrosion [52,53]. The sub mechanism is expected to vary based on the surface processing conditions that tends to affect the particle generated during tribocorrosion [54,55]. Studies have shown that abrasive wear particles can vary in size based on the surface characteristics [6,22,53]. The varying size of wear particles generated as a function of laser intensity (that dictates the surface characteristic) causes reaction products to be formed at different rates during tribocorrosion [56,57]. The adhered particles can include reaction products and/or wear particles (size depends on surface processing) from to the substrate that can lead to a third body abrasive wear, changes the wear behavior as result of wear and corrosion synergy [53]. Depending on the characteristics of the reaction products and wear particles interacting as a third -body, the wear behavior can vary drastically as observed from untreated AZ31B surface to the LSP treated.

With increase in laser intensity, SR also increases (Fig. 3), which increases the exposed real surface area to corrosive environment during wear, initiating the wear-corrosion synergism. The dominant surface hardening effect of LSP at low laser intensities enhances the surfaces properties to have increased wear-corrosion synergistic resistance [6]. Whereas, an increase in wear accelerated corrosion is observed due to a dominant surface roughening effect at high laser intensities [6]. This behavior of LSP processed surface was clear from the results where, LSP-1 processing increased the hardness by 5.1% and reduced the wear volume by 66.4%. LSP-2 processing increased the hardness by 7% and reduced the wear volume by 61.7%. LSP-3 processing increased the hardness by 10% and reduced the wear volume by 58.7%. LSP-4 processing increased the hardness by 11.8% and reduced the wear volume by 50%. LSP-5 processing increased the hardness by 15% and reduced the wear volume by 37.8%. Theoretically, the hardness is expected to increase with a decrease in the corresponding wear volume, as the laser intensity increases. But the results show that after LSP-3 the increase in hardness does not translate to decrease in wear volume [22].

Studies on the wear mechanism observed during tribocorrosion of LSP processed AZ31B surfaces have shown that the wear particles of micron to sub-micron size are generated during sliding [58]. The size and amount of the wear particles generated are dependent on the laser intensity used to process the AZ31B surfaces. The generated particles then define a three-body wear mechanism during sliding that is susceptible to corrosion and further accelerate the wear under the influence of tribocorrosion [22].

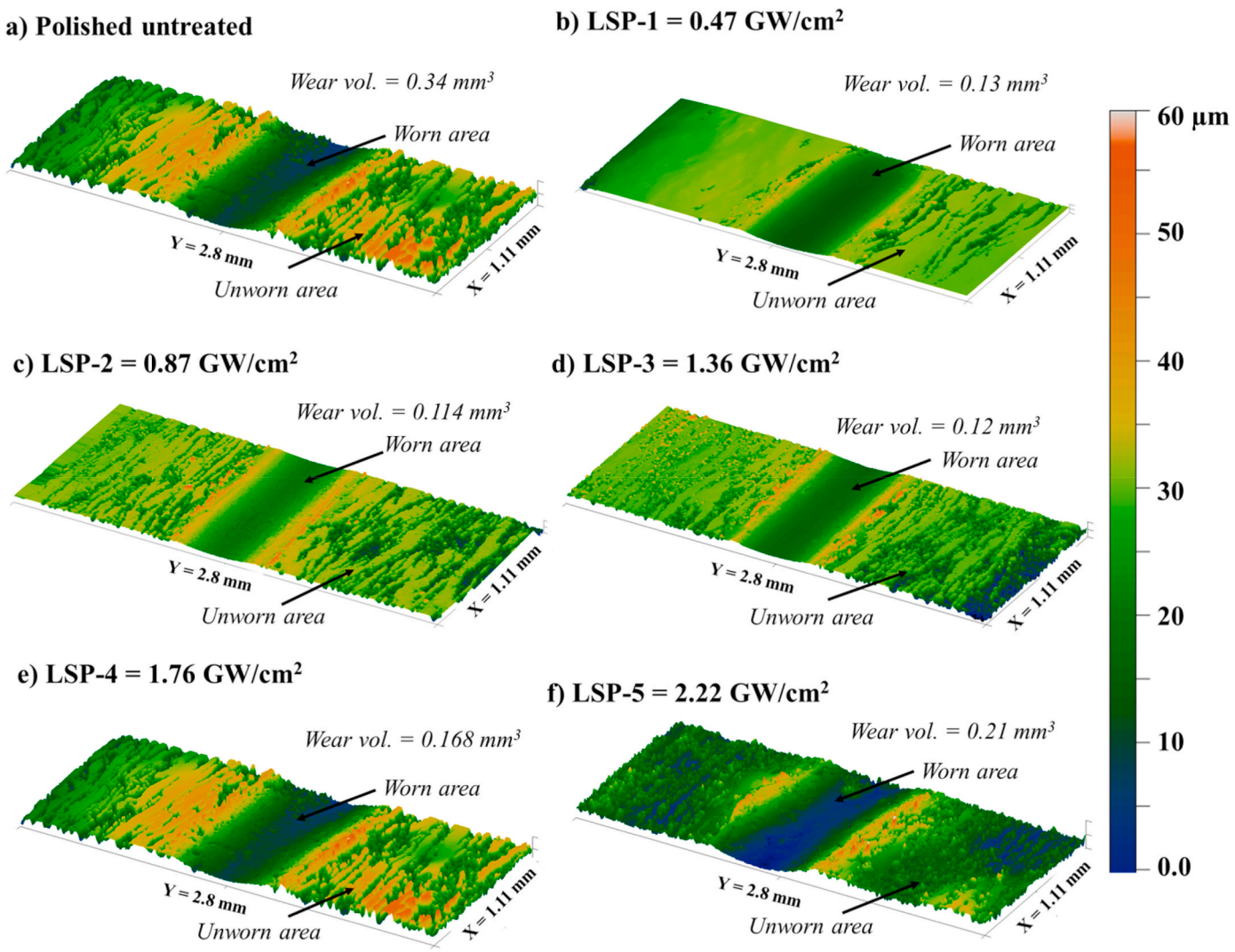

Fig. 8. Wear track profiles after tribocorrosion testing on AZ31B treated at different laser intensities (a–f).

3.3. Influence of LSP and tribocorrosion on SR

During the tribocorrosion set of experiments, sliding was initiated only after ensuring a stable OCP within the tribochemical system was achieved over 1 h. It was observed that all LSP processed surfaces (LSP-1 to LSP-5) stabilized at a potential of -1.59 ± 0.008 V except for the untreated surface, which stabilized at a slightly higher potential of -1.538 ± 0.005 V. The cathodic potential was applied at 1 V below these OCP values to measure wear without corrosion during the tribocorrosion tests. To understand the influence of SR in defining the wear mechanism on LSP processed surfaces, the variation in SR and wear volume due to tribocorrosion was investigated. The SR, wear track, and area around the wear track was recorded post tribocorrosion testing on each LSP surface using 3D optical profilometer. All tribocorroded surfaces were compared against their respective SR and wear tracks on LSP processed (LSP-1 to LSP-5), and untreated surface (LSP-0, Untreated) of AZ31B. The observed values of SR parameters S_a, S_p, S_v, S_z, and change in surface area after tribocorrosion on LSP surfaces are reported in Table 3. Results show that the change in SR due to tribocorrosion on LSP processed surfaces can be best perceived using S_a and S_z roughness parameters [22].

The plots comparing the change in SR parameters and surface area of LSP processed and tribocorroded LSP surfaces are shown in Fig. 6. The linear trend of SR observed for LSP processing (Fig. 6a) on AZ31B did not hold true after the surfaces experienced tribocorrosion. It can be observed in Fig. 6b, that tribocorrosion has a drastic effect on SR, where LSP-1 surface underwent the least change (9.0%), and LSP-0 (untreated) surface underwent the highest change (31.9%) as compared to their respective conditions before tribocorrosion (Fig. 6a). The results show that the surface treated with LSP-1 could resist surface degradation better than any other surfaces tested in this study, indicating that low laser intensity treated surfaces can resist mechanochemical degradation effects of tribocorrosion better than untreated or surface treated with high laser intensities [6,22]. The variations in asperity height and surface properties of LSP surfaces post tribocorrosion has been shown to be a combination of wear, corrosion, and wear-corrosion synergistic degradation [22].

In environments susceptible to corrosion and tribocorrosion, SR and S_E play an important role. S_E defines how easy or difficult it is for a surface to interact with various fluids on a molecular scale and thus defines the wettability of a solid surface. The SR can drastically modify the S_E by affecting the surface area and wetting behavior. This effect of SR further translates into the modification of electrochemical interactions at the interface of the surface and aqueous media that affects the tribocorrosion properties for AZ31B Mg alloy.

The effect of SR in defining the wear mechanism on LSP processed surfaces can be further understood by studying the wear tracks and the area around the wear track. The wear tracks without the influence of

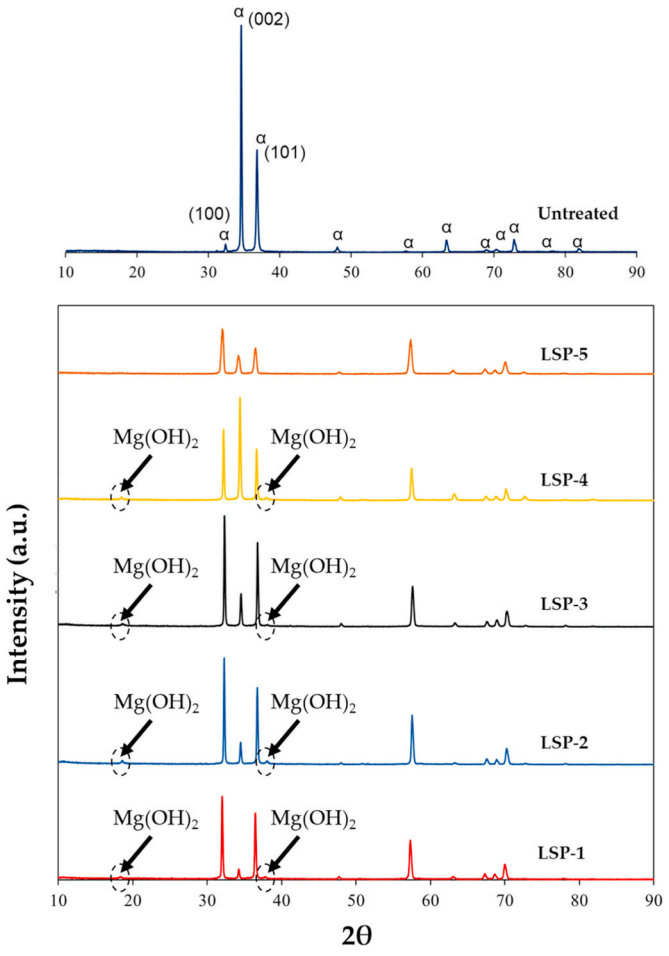

Fig. 9. XRD of LSP processed surfaces after tribocorrosion.

corrosion on LSP processed AZ31B surfaces (cathodically polarized) are shown in Fig. 7. It was observed that there was negligible change in the area around the wear track hence Fig. 7 depicts the wear track generated due to sliding without tribocorrosion. When sliding occurs on the LSP processed AZ31B surfaces under the influence of tribocorrosion, there was a drastic increase in the wear depth and SR around the wear tracks, as shown in Fig. 8. The mechanism of wear for AZ31B during tribocorrosion depends on pitting [59], and galvanic corrosion formed as a result of differential electrocatalytic mechanism [22,60,61]. The localized corrosion on the unworn regions in combination with the worn area forms a galvanic couple due to the change in their galvanic potentials after the initiation of pitting corrosion. The surface morphology of these galvanic couples can be very distinctly depending on the applied laser intensity (Fig. 8) and wear under the influence of corrosion. The degradation effect of tribocorrosion on the SR of the unworn regions is also evident in Fig. 8. These mechanochemical degradations on the AZ31B Mg surface modify the SR based on laser intensity during LSP and their susceptibility to tribocorrosion.

The start of corrosion on the unworn areas in the 0.6 M NaCl aqueous medium causes pits which result from the breakdown of oxide film during LSP [59]. A similar trend around the wear tracks in Fig. 8 was observed. The thin oxide film on the AZ31B surfaces was characterized using normal X-ray diffraction (XRD), and the X-ray diffractogram was obtained, as shown in Fig. 9. It was clear that a magnesium hydroxide ($Mg(OH)_2$) layer was present on surfaces of LSP-1 to LSP-4. The layer was not detected in the case of the untreated surface and LSP-5. This indicates a weak oxide layer with respect to the pit propagation and that there is a limit to the resilience of the oxide film, which depends on the applied laser intensity. The untreated surface showed the most pitting

Table 4
Contact angle measurements of LSP processed AZ31B surfaces before and after tribocorrosion.

Test condition	Contact angle (θ)			Surface roughness (S_a, μm)
	Water (W)	0.6 M NaCl (N)	Glycerol (G)	
Untreated	74.5	87.06	75.25	0.3 ± 0.08
After tribocorrosion	53.31	54.41	73.78	3.2 ± 0.18
LSP-1	72.24	69.16	78.6	0.35 ± 0.02
After tribocorrosion	74.12	59.89	64.93	1.36 ± 0.1
LSP-2	77.8	74.78	74.16	0.45 ± 0.02
After tribocorrosion	58.5	37.42	38.61	1.7 ± 0.15
LSP-3	85.22	83.15	80.39	0.5 ± 0.05
After tribocorrosion	63.45	32.55	35.12	2.21 ± 0.13
LSP-4	85.54	80.68	75.05	0.6 ± 0.05
After tribocorrosion	68.77	39.65	52.06	2.7 ± 0.8
LSP-5	78.19	72.03	65.9	0.9 ± 0.06
After tribocorrosion	76.53	70.53	66.06	1.5 ± 0.1

due to the presence of a weak oxide layer followed by LSP-5 surface, where the high laser intensity is expected to have similar effects. The surface pit morphology and distribution were assessed using the 3D optical profilometer, as seen in Fig. 8. The LSP at low laser intensities, especially LSP-1, was found to strengthen the oxide layer increasing its resilience to pitting corrosion and hence tribocorrosion. At high laser intensity, it is expected that the high shock peening effect weakens the oxide layer making the surface susceptible to pitting. Additionally, pitting was also evident on the wear tracks of the untreated surface and surfaces treated at high laser intensity (LSP 3 to LSP 5), as seen in Fig. 8. Studies have indicated that laser-based surface treatments can result in the formation of a more stable Mg(OH)2 layer [62]. This is evident from the surface energy change in the present study involving LSP processed surfaces and the absence of the layer on untreated surface.

These results indicate that LSP modifies the SR in addition to surface characteristics and thus, causes a change in the resilience of the surface to tribocorrosion. Since S_E and wettability of a solid are driven by SR, it is necessary to understand the tribocorrosion behavior of LSP processed AZ31B Mg surfaces as a function of the SR and S_E. Even though the influence of LSP processing on the tribocorrosion susceptibility of AZ31B has been investigated [22], the repercussions of tribocorrosion on the S_E of LSP processed area has not been well understood. Investigating the influence of LSP on S_E requires the wear after tribocorrosion to be studied considering the change in SR and S_E due to LSP.

3.4. Influence of LSP on contact angle and tribocorrosion

The surface characteristics, such as SR and S_E, define the interfacial area and wettability of a solid surface in aqueous environments. The interaction of the solid surface with the aqueous environment dictates the corrosion and tribocorrosion inhibition properties of surface treatments such as LSP. In the present study, the total S_E and the solid-liquid interfacial S_E of LSP processed AZ31B Mg surface with probe liquids (Table 2) – water (W), 0.6 M NaCl (N), and glycerol (G) was calculated through sessile droplet contact angle measurement method (ASTM D7334 - 08 (2013)). The total S_E was calculated based on the three-component approach developed by Van Oss et al. [25,26]. The change in contact angles due to tribocorrosion on the LSP processed AZ31B surface is shown in Table 4. The LSP processed surfaces had a high contact angle due to low SR as compared to the tribocorroded LSP surfaces. Low contact angles indicated easy wetting (liquid adhesion) of the surface that increases the contact area of the surface with liquids and thus its susceptibility to corrosion.

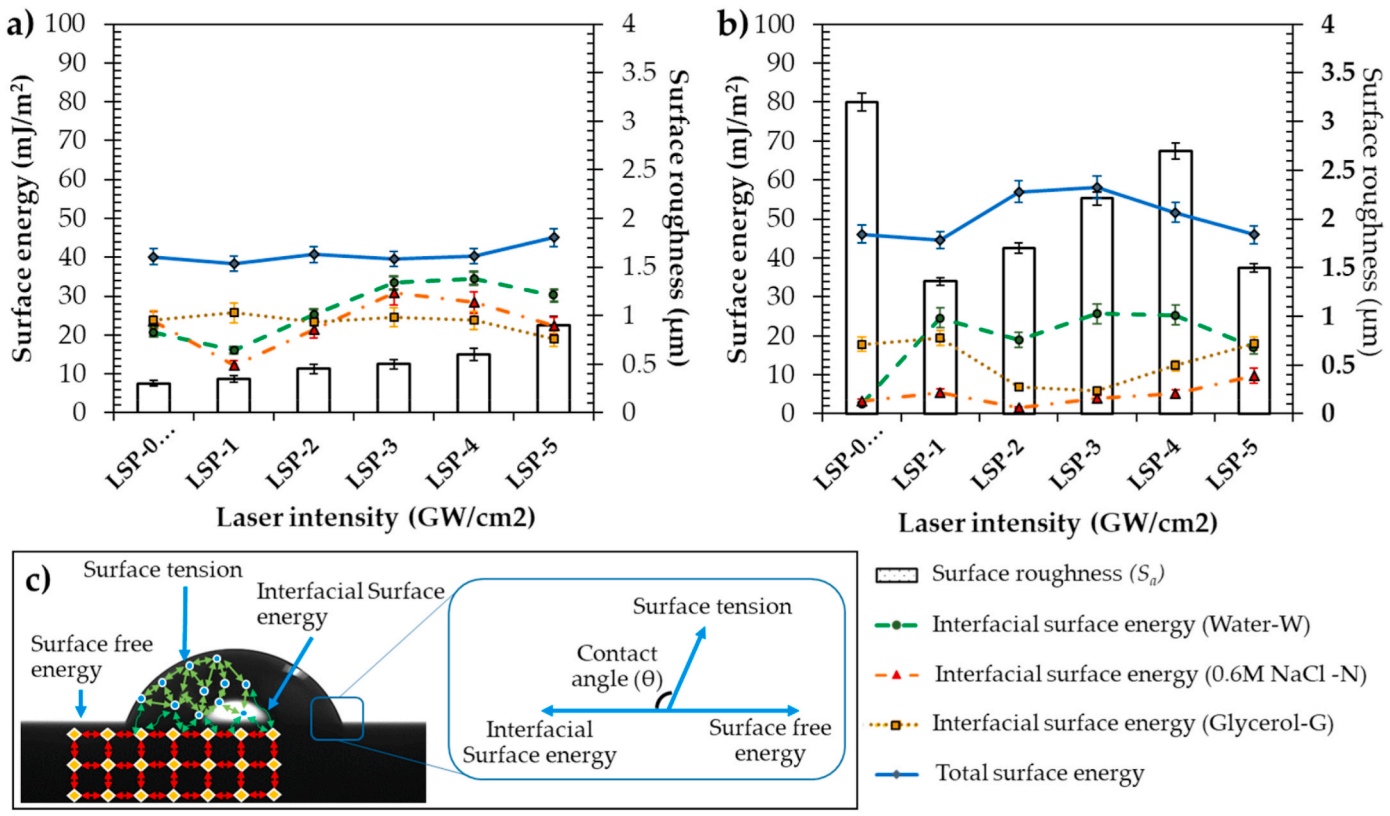

Fig. 10. Surface energy of (a) LSP processed AZ31B surface and (b) tribocorroded LSP processed AZ31B surface. (c) Schematic representation of surface energy of solid (surface free energy), surface tension of liquid, the interfacial surface energy between the solid and liquid, and the resulting contact angle (θ).

The tribocorroded surfaces had the lowest contact angles when in interface with 0.6 M NaCl as compared to the interfaces with water and glycerol. This is due to the high polar and corrosive nature of aq. NaCl that causes an increase in the liquid adhesion corresponding to the S_E of the solid. It is this behavior of AZ31B surface, which makes its use limited in aqueous environments, and susceptible to corrosion and tribocorrosion. However, the contact angle measurements indicate that LSP processing can modify the SR to increase the contact angle at the interface of AZ31B surface and aqueous mediums. Additionally, LSP is observed to increase the resilience of the surface to tribocorrosion, where it was observed that the surface could maintain a relatively high contact angle even after experiencing tribocorrosion.

3.5. *Influence of LSP on S_E and tribocorrosion*

The contact angles (Table 4) and the surface tension data of the probe liquids (Table 2) were used to calculate the total S_E and the solid-liquid interfacial S_E of each LSP processed AZ31B surface. The total and the interfacial S_E were calculated for LSP processed surfaces and compared with the resulting surface energies post tribocorrosion, as shown in Fig. 10. It can be observed that the total S_E increases after tribocorrosion for all surfaces, indicative of the surface degradation and change in SR due to tribocorrosion. The increase in S_E post tribocorrosion indicates an increased adhesion of the liquid to the surface. The surface processed at LSP-1 experiences the least change in total S_E and has the lowest S_E after tribocorrosion, while LSP-3 had the highest change in S_E due to tribocorrosion. It can be observed in Fig. 10a that even though the total S_E of the untreated and LSP processed surface is almost the same, within a range of 38–45 mJ/m^2, the solid-liquid interfacial S_E with various probe liquids varies considerably. The untreated surface exhibits minimal variation in the interfacial S_E irrespective of the probe liquid, whereas the surfaces after LSP exhibit a considerable change in interfacial S_E due to the evolution of physical attributes, specifically SR [42,63].

Fig. 10b shows the LSP processed surfaces under the influence of tribocorrosion experience an increase in total S_E. This is due to the initiation and propagation of pitting corrosion that increases SR. The total S_E is observed to increase with an increase in laser intensity, but at high laser intensity (LSP-4 and LSP-5), it has been shown that the shock peening influence of LSP is high enough to restructure (plastic deformation) the surface asperities [6]. At high laser intensities, the asperities are plastically deformed to have small sharp asperities, results in lower mean SR. This decrease in SR due to LSP at high laser intensity increases the resilience to tribocorrosion as there is a decrease in the area prone to galvanic corrosion during wear. Hence, a decrease in S_E is observed after tribocorrosion on high laser intensity processed surfaces (LSP-4 and 5). It has been shown that when a pitting form of corrosion initiates and degrades the surface, the SR increases, causing a decrease in S_E and an increase in the adhesion of the liquid to the surface [42]. Hence, the change in S_E of LSP processed surfaces after tribocorrosion is attributed to the evolution of mechanochemical degradation such as wear, corrosion, and tribocorrosion.

The solid-liquid interfacial S_E of the untreated and LSP processed surfaces with the probe liquids, observed in Fig. 10, decreases after tribocorrosion except for LSP-1. In the case of LSP-1, the interfacial S_E with water increases after tribocorrosion due to pockets of air being trapped at the interface. The pockets of air trapped at the interface are because of relatively low surface degradation and minimal change in SR after tribocorrosion. However, when the LSP-1 is in contact with 0.6 M NaCl, the interfacial energy decreases due to the increased polar interactions. This causes the air pockets to collapse. The decrease in interfacial energy in the case of remaining LSP surfaces is due to similar reasons (Fig. 10). The LSP increases the SR as a function of laser intensity that causes more air to be trapped at the interface, which increases the interfacial S_E. The change in SR after LSP was found to be insufficient to cause a significant effect on the interfacial energies with the standard probe liquid-glycerol.

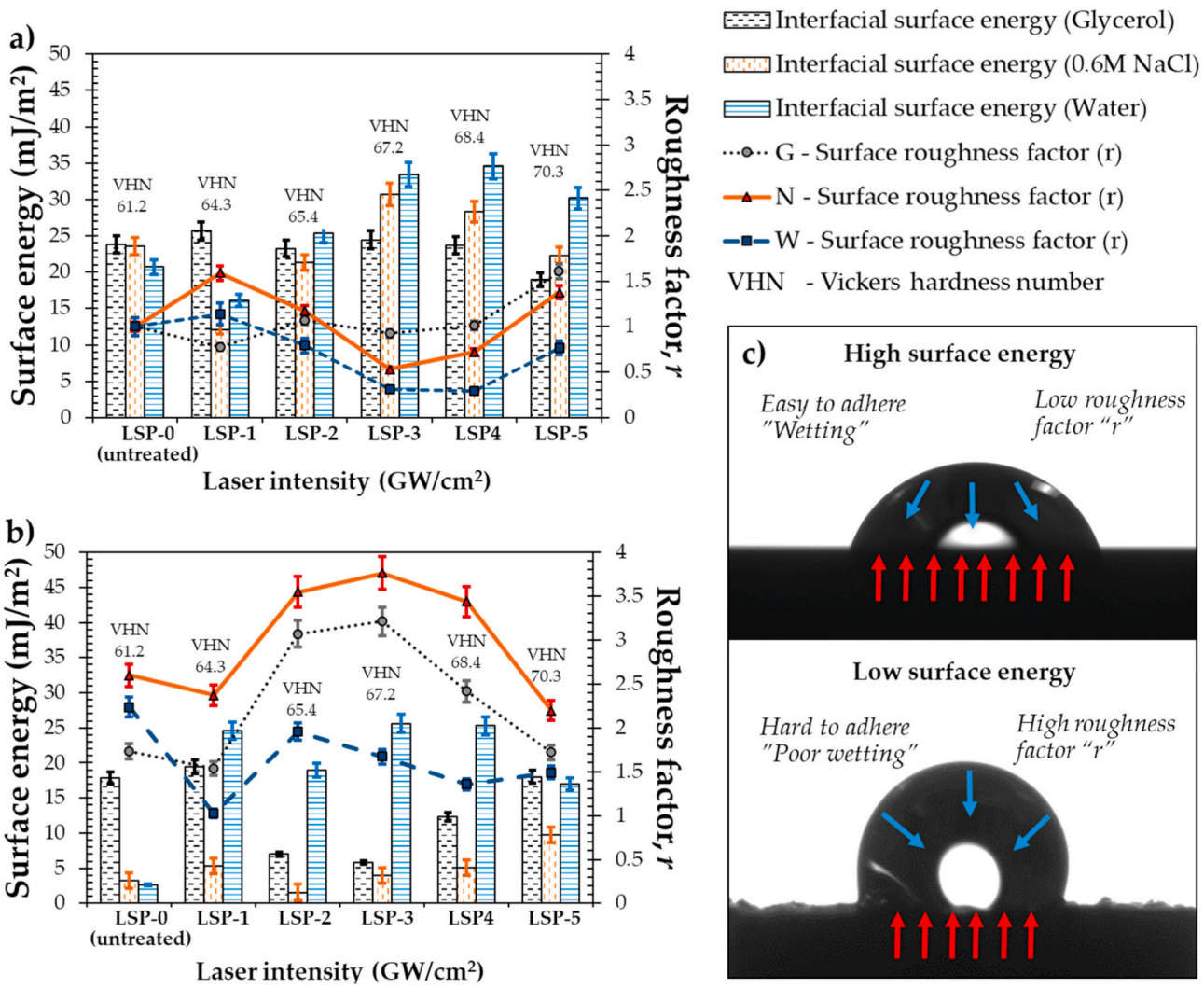

Fig. 11. Surface roughness factor calculated with respect to the untreated surface condition for (a) LSP processed AZ31B and (b) tribocorroded LSP processed AZ31B surface. (c) Schematic representation of the correlation between the roughness factor and wetting due to the interfacial S_E.

Further, after tribocorrosion, the drastic increase in SR combined with the oxide layer break down causes the interfacial S_E to decrease. This insight into the interfacial S_E shows that even though the total S_E of the LSP processed surfaces increase after tribocorrosion, their interfacial S_E are defined by the SR and polar interactions at the solid-liquid interface. These results indicate that the observed surface degradation due to galvanic corrosion is accelerated by wear in a corrosive environment such as 0.6 M NaCl and depends on the interfacial S_E of solid with the aqueous environment.

3.6. Effect of SR on interfacial S_E and tribocorrosion

The wetting behavior of a solid surface depend on the SR [64]. The SR affecting the wetting behavior is defined as the ratio of actual to geometric surface area and cannot be quantified by mapping the surface profiles. In order to correlate the variation of SR caused by the initiation of tribocorrosion to the S_E, Wenzel wetting model was applied. Wenzel [65] defined a roughness factor *r,* which was the ratio of the actual surface area to geometric surface. This factor *r* can be considered in the Young's equation as:

$$r(\gamma_s - \gamma_{sl}) = \gamma_l \cos\theta$$

where, $r = \frac{\text{actual surface area}}{\text{geometric surface area}}$

The *r* values were calculated as shown in Fig. 11, considering the *actual surface area* as the untreated surface (LSP-0, before tribocorrosion), and the *geometric surface area* as the surface area after LSP (Fig. 11a), and LSP surfaces undergoing tribocorrosion (Fig. 11b). These *r* values were calculated for each probe liquid to understand the effect of SR on the interfacial S_E at the solid-liquid interface. The *r* value is an indicative of the resilience imbibed by LSP processing to tribocorrosion through the modification SR and surface characteristics. It can be observed in Fig. 11a that the referenced untreated surface (LSP-0, before tribocorrosion) has an *r* value of 1 with all probe liquids, indicating the ideal condition (*actual surface area*) of the SR. As the interfacial S_E decreases, the *r* value increases, and vice versa, this indicates that influence of LSP on SR followed by effect of tribocorrosion on wetting behavior of the surfaces (Fig. 11c). Comparing the roughness ratio for LSP processed (Fig. 11a) and tribocorroded LSP surfaces (Fig. 11b), it can be observed that the least change in *r* was for LSP-1 surface. This characteristic of LSP-1 is an indicative of the optimum surface characteristics obtained through LSP. A minimal change in *r* value shows that the surface characteristics are retained even after experiencing tribocorrosion. Hence, low S_E was observed for LSP-1 even after tribocorrosion (Fig. 10b) indicative of enhanced corrosion and tribocorrosion resistance [6,22].

A large change in *r* value was observed for samples LSP-2, LSP-3 and LSP-4. It occurs because of an increase in SR after LSP, which causes an

increase in the surface area exposed to tribocorrosion. The increase in r value and decrease in solid-liquid interfacial S_E after tribocorrosion for LSP-2 to LSP-4 indicates the high susceptibility of these surfaces to tribocorrosion. Even though theoretically, the wetting should be poor when a high r value is observed, under the influence of tribocorrosion, the high r values can be detrimental since they indicate an increase in surface area. In the case of surface processed at LSP-5, due to the high laser intensity, the surface asperities undergo a large degree of plastic deformation during LSP processing, which results in small sharp asperities reducing the mean roughness [6]. Hence, a low gradient change in r value and interfacial S_E is observed for LSP-5 after tribocorrosion. Even though this characteristic of LSP-5 is similar to the LSP-1 surface, the LSP-5 experiences a higher degree of surface degradation than LSP-1. This is due to the absence of an oxide layer (Fig. 9), which leads to a change in S_E after tribocorrosion.

4. Conclusions

The influence of LSP on S_E and the onset of tribocorrosion was investigated on the AZ31B surfaces. Contact angle measurements were made on LSP processed surfaces and tribocorroded LSP surfaces according to the standard practice detailed under ASTM D7334 - 08 (2013). The study uses a three-component approach based on Lewis acid-base surface interaction components to understand the S_E interactions. Liquids, namely, distilled water (W), Glycerol (G), and 0.6 M NaCl (N), were used in the contact angle measurements. These liquids, specifically water and 0.6 M NaCl, simulate some of the atmospheric conditions which dictate the corrosion properties of surfaces. The following are the conclusions resulting from this investigation:

- Low laser LSP (LSP-1) reduced the wear under the influence of corrosion by more than three times as compared to the untreated surface.
- Surface degradation due to corrosion is accelerated by wear in a corrosive environment and depends on the interfacial S_E of solid with the aqueous environment.
- LSP-1 experienced the least change (9.0%) in surface roughness after tribocorrosion, and the untreated surface experienced the highest change in surface roughness at 31.9%.
- The change in surface roughness and liquid adhesion (wettability) due to LSP modifies the solid-liquid interfacial S_E that depends on applied laser intensity.
- A negligible change in the roughness factor (r) is observed after tribocorrosion for low laser intensity treated surfaces which shows the resilience of LSP to tribocorrosion.
- The solid-liquid interfacial S_E of the untreated and LSP processed surface decreases after tribocorrosion except for LSP-1.
- Magnesium hydroxide ($Mg(OH)_2$) layer was present on surfaces treated from LSP-1 to LSP-4 in decreasing order of $Mg(OH)_2$ peak intensity post tribocorrosion. The high peak intensity of $Mg(OH)_2$ indicated better tribocorroion resistance.
- The $Mg(OH)_2$ layer was not detected in the case of the untreated surface and LSP-5 post tribocorrosion.
- LSP processed surfaces exhibit a high contact angle due to a decrease in interfacial S_E.
- The LSP processed surfaces have a relatively high contact angle (low wettability) in aqueous environments post tribocorrosion as compared to the untreated surface.
- The total S_E of the AZ31B increases after the LSP processed surface undergo tribocorrosion.
- The increase in S_E post tribocorrosion can be attributed to the evolution of mechanochemical attributes.

Declaration of competing interest

The authors declare that they have no known competing financial interests or personal relationships that could have appeared to influence the work reported in this paper.

Acknowledgment

The authors are thankful for the startup funds provided as financial support by the Dept. Of Mechanical Eng. At the University of Nevada, Reno.

References

[1] V. Tibrewal, K. Dak, A. Himanshu, H. Kumar, P. Kuppan, A.S.S. Balan, Cryogenic machining of AZ31B magnesium alloy for bio-implant applications, in: Advances in Forming, Machining and Automation, Springer, 2019, pp. 239–251.
[2] S. Wu, Z. Ji, T. Zhang, Microstructure and mechanical properties of AZ31B magnesium alloy recycled by solid-state process from different size chips, J. Mater. Process. Technol. 209 (2009) 5319–5324.
[3] Z. Pu, G.L. Song, S. Yang, J.C. Outeiro, O.W. Dillon, D.A. Puleo, I.S. Jawahir, Grain refined and basal textured surface produced by burnishing for improved corrosion performance of AZ31B Mg alloy, Corrosion Sci. 57 (2012) 192–201.
[4] Y. Liu, S. Cai, L. Dai, A new method for grain refinement in magnesium alloy: High speed extrusion machining, Mater. Sci. Eng., A 651 (2016) 878–885.
[5] B. Mao, A. Siddaiah, P.L. Menezes, Y. Liao, Surface texturing by indirect laser shock surface patterning for manipulated friction coefficient, J. Mater. Process. Technol. 257 (2018) 227–233.
[6] A. Siddaiah, B. Mao, Y. Liao, P.L. Menezes, Surface characterization and tribological performance of laser shock peened steel surfaces, Surf. Coating. Technol. 351 (2018) 188–197.
[7] B. Mao, Y. Liao, B. Li, Gradient twinning microstructure generated by laser shock peening in an AZ31B magnesium alloy, Appl. Surf. Sci. 457 (2018) 342–351.
[8] B. Mao, B. Li, D. Lin, Y. Liao, Enhanced room temperature stretch formability of AZ31B magnesium alloy sheet by laser shock peening, Mater. Sci. Eng., A 756 (2019) 219–225.
[9] X. Zhang, B. Mao, A. Siddaiah, P.L. Menezes, Y. Liao, Direct laser shock surface patterning of an AZ31B magnesium alloy: microstructure evolution and friction performance, J. Mater. Process. Technol. 275 (2020) 116333.
[10] Y.M. Baqer, S. Ramesh, F. Yusof, S.M. Manladan, Challenges and advances in laser welding of dissimilar light alloys: Al/Mg, Al/Ti, and Mg/Ti alloys, Int. J. Adv. Manuf. Technol. 95 (2018) 4353–4369.
[11] J. Chen, L. Tan, X. Yu, I.P. Etim, M. Ibrahim, K. Yang, Mechanical properties of magnesium alloys for medical application: A review, Journal of the Mechanical Behavior of Biomedical Materials 87 (2018) 68–79.
[12] D. Carou, E.M. Rubio, J.P. Davim, Machinability of magnesium and its alloys: A review, in: J.P. Davim (Ed.), Traditional Machining Processes: Research Advances, Springer Berlin Heidelberg, Berlin, Heidelberg, 2015, pp. 133–152.
[13] P. Wan, L. Tan, K. Yang, Surface modification on biodegradable magnesium alloys as orthopedic implant materials to improve the bio-adaptability: A review, J. Mater. Sci. Technol. 32 (2016) 827–834.
[14] J. Wang, X. Pang, H. Jahed, Surface protection of Mg alloys in automotive applications: A review, AIMS Materials Science 6 (2019) 567–600.
[15] D. Zhao, F. Witte, F. Lu, J. Wang, J. Li, L. Qin, Current status on clinical applications of magnesium-based orthopaedic implants: A review from clinical translational perspective, Biomaterials 112 (2017) 287–302.
[16] C. Blawert, W. Dietzel, E. Ghali, G. Song, Anodizing treatments for magnesium alloys and their effect on corrosion resistance in various environments, Adv. Eng. Mater. 8 (2006) 511–533.
[17] R. Zeng, W. Dietzel, F. Witte, N. Hort, C. Blawert, Progress and challenge for magnesium alloys as biomaterials, Adv. Eng. Mater. 10 (2008) B3–B14.
[18] S.A. Salman, M. Okido, 8 - anodization of magnesium (Mg) alloys to improve corrosion resistance, in: G.-L. Song (Ed.), Corrosion Prevention of Magnesium Alloys, Woodhead Publishing, 2013, pp. 197–231.
[19] H.M. Mousa, C.H. Park, C.S. Kim, Surface modification of magnesium and its alloys using anodization for orthopedic implant application, Magnesium Alloys (2017) 219.
[20] T.C. Wu, Y.H. Ho, S.S. Joshi, R.S. Rajamure, N.B. Dahotre, Microstructure and corrosion behavior of laser surface-treated AZ31B Mg bio-implant material, Laser Med. Sci. 32 (2017) 797–803.
[21] R. Zhang, X. Zhou, H. Gao, S. Mankoci, Y. Liu, X. Sang, H. Qin, X. Hou, Z. Ren, G. L. Doll, A. Martini, Y. Dong, N. Sahai, C. Ye, The effects of laser shock peening on the mechanical properties and biomedical behavior of AZ31B magnesium alloy, Surf. Coating. Technol. 339 (2018) 48–56.
[22] A. Siddaiah, B. Mao, Y. Liao, P.L. Menezes, Effect of laser shock peening on the wear-corrosion synergistic behavior of AZ31B magnesium alloys, J. Tribol. (2019) 1–22.
[23] B. Mao, A. Siddaiah, X. Zhang, B. Li, P.L. Menezes, Y. Liao, The influence of surface pre-twinning on the friction and wear performance of an AZ31B Mg alloy, Appl. Surf. Sci. 480 (2019) 998–1007.
[24] M.-Z. Ge, J.-Y. Xiang, L. Yang, J.T. Wang, Effect of laser shock peening on the stress corrosion cracking of AZ31B magnesium alloy in a simulated body fluid, Surf. Coating. Technol. 310 (2017) 157–165.
[25] C.J. van Oss, M.K. Chaudhury, R.J. Good, Monopolar surfaces, Adv. Colloid Interface Sci. 28 (1987) 35–64.

[26] C.J. Van Oss, M.K. Chaudhury, R.J. Good, Interfacial Lifshitz-van der Waals and polar interactions in macroscopic systems, Chem. Rev. 88 (1988) 927–941.
[27] B.-Q. Fu, W. Liu, Z.-L. Li, Calculation of the surface energy of hcp-metals with the empirical electron theory, Appl. Surf. Sci. 255 (2009) 9348–9357.
[28] S.K. Behera, A. Kumar P, N. Dogra, M. Nosonovsky, P. Rohatgi, Effect of microstructure on contact angle and corrosion of ductile iron: iron–graphite composite, Langmuir 35 (2019) 16120–16129.
[29] C.S. Montross, T. Wei, L. Ye, G. Clark, Y.-W. Mai, Laser shock processing and its effects on microstructure and properties of metal alloys: A review, Int. J. Fatig. 24 (2002) 1021–1036.
[30] H. Wang, C. Ning, Y. Huang, Z. Cao, X. Chen, W. Zhang, Improvement of abrasion resistance in artificial seawater and corrosion resistance in NaCl solution of 7075 aluminum alloy processed by laser shock peening, Optic Laser. Eng. 90 (2017) 179–185.
[31] P. Shukla, S. Nath, G. Wang, X. Shen, J. Lawrence, Surface property modifications of silicon carbide ceramic following laser shock peening, J. Eur. Ceram. Soc. 37 (2017) 3027–3038.
[32] H. Wang, Y. Huang, W. Zhang, A. Ostendorf, Investigation of multiple laser shock peening on the mechanical property and corrosion resistance of shipbuilding 5083Al alloy under a simulated seawater environment, Appl. Optic. 57 (2018) 6300–6308.
[33] J. Dutta Majumdar, R. Galun, B.L. Mordike, I. Manna, Effect of laser surface melting on corrosion and wear resistance of a commercial magnesium alloy, Mater. Sci. Eng., A 361 (2003) 119–129.
[34] I. Yakimets, C. Richard, G. Béranger, P. Peyre, Laser peening processing effect on mechanical and tribological properties of rolling steel 100Cr6, Wear 256 (2004) 311–320.
[35] A. Kulkarni, S. Chettri, S. Prabhakaran, S. Kalainathan, Effect of laser shock peening without coating on surface morphology and mechanical properties of nickel-200, mechanics, Materials Science & Engineering MMSE Journal 9 (2017). Open Access.
[36] F. Dai, J. Zhou, J. Lu, X. Luo, A technique to decrease surface roughness in overlapping laser shock peening, Appl. Surf. Sci. 370 (2016) 501–507.
[37] V.D. Ta, A. Dunn, T.J. Wasley, J. Li, R.W. Kay, J. Stringer, P.J. Smith, E. Esenturk, C. Connaughton, J.D. Shephard, Laser textured surface gradients, Appl. Surf. Sci. 371 (2016) 583–589.
[38] L. Petan, J.L. Ocaña, J. Grum, Effects of laser shock peening on the surface integrity of 18 % Ni maraging steel, Strojniški vestnik - Journal of Mechanical Engineering 62 (5) (2016), https://doi.org/10.5545/sv-jme.2015.3305(2016). Strojniški vestnik - Journal of Mechanical EngineeringDO -.
[39] F.Z. Dai, Z.D. Zhang, J.Z. Zhou, J.Z. Lu, Y.K. Zhang, Analysis of surface roughness at overlapping laser shock peening, Surf. Rev. Lett. 23 (2016) 1650012.
[40] D.V. Ta, A. Dunn, T.J. Wasley, R.W. Kay, J. Stringer, P.J. Smith, C. Connaughton, J. D. Shephard, Nanosecond laser textured superhydrophobic metallic surfaces and their chemical sensing applications, Appl. Surf. Sci. 357 (2015) 248–254. Part A.
[41] V.D. Ta, A. Dunn, T.J. Wasley, J. Li, R.W. Kay, J. Stringer, P.J. Smith, E. Esenturk, C. Connaughton, J.D. Shephard, Laser textured superhydrophobic surfaces and their applications for homogeneous spot deposition, Appl. Surf. Sci. 365 (2016) 153–159.
[42] Y.-H. Ho, H.D. Vora, N.B. Dahotre, Laser surface modification of AZ31B Mg alloy for bio-wettability, J. Biomater. Appl. 29 (2014) 915–928.
[43] N. Epperlein, F. Menzel, K. Schwibbert, R. Koter, J. Bonse, J. Sameith, J. Krüger, J. Toepel, Influence of femtosecond laser produced nanostructures on biofilm growth on steel, Applied Surface Science $V 418 (2017) 420–424.
[44] A. Singh, D.S. Patel, J. Ramkumar, K. Balani, Single step laser surface texturing for enhancing contact angle and tribological properties, Int. J. Adv. Manuf. Technol. 100 (2019) 1253–1267.
[45] L. Romoli, F. Moroni, M.M.A. Khan, A study on the influence of surface laser texturing on the adhesive strength of bonded joints in aluminium alloys, CIRP Ann. - Manuf. Technol. 66 (2017) 237–240.
[46] B.E. Rapp, Chapter 22 - measuring surface tension and free surface energy, in: B. E. Rapp (Ed.), Microfluidics: Modelling, Mechanics and Mathematics, Elsevier, Oxford, 2017, pp. 453–465.
[47] P.L. Menezes, S.P. Ingole, M. Nosonovsky, S.V. Kailas, M.R. Lovell, Tribology for Scientists and Engineers, Tribology for Scientists and Engineers, Springer, 2013, pp. 9–28.
[48] R. Zhang, X. Hou, X. Zhou, H. Gao, S. Mankoci, H. Qin, Z. Ren, G.L. Doll, A. Martini, Y. Dong, N. Sahai, C. Ye, Effects of Laser Shock Peening on the Wear and Degradation Behaviors of Magnesium Alloys, 2016. V002T001A005.
[49] S. Prabhakaran, A. Kulkarni, G. Vasanth, S. Kalainathan, P. Shukla, V. K. Vasudevan, Laser shock peening without coating induced residual stress distribution, wettability characteristics and enhanced pitting corrosion resistance of austenitic stainless steel, Appl. Surf. Sci. 428 (2018) 17–30.
[50] H. Kawahara, Oral Implantology and Biomaterials: Proceedings of the 3rd International Congress of Implantology and Biomaterials in Stomatology, Elsevier Science Ltd, 1989. Osaka, April 27-29, 1988.
[51] L. Feenstra, K. de Groot, Medical Use of Calcium Phosphate Ceramics, Bioceramics of calcium phosphate, 1983, pp. 131–141.
[52] K.H. Zum Gahr, Microstructure and Wear of Materials, Elsevier, 1987.
[53] A.I. Muñoz, N. Espallargas, Tribocorrosion Mechanisms in Sliding Contacts, Tribocorrosion of Passive Metals and Coatings, Elsevier, 2011, pp. 118–152.
[54] D. Sun, J.A. Wharton, R.J.K. Wood, Micro-abrasion–corrosion of cast CoCrMo—effects of micron and sub-micron sized abrasives, Wear 267 (2009) 52–60.
[55] M.N. Rahaman, A. Yao, B.S. Bal, J.P. Garino, M.D. Ries, Ceramics for prosthetic hip and knee joint replacement, J. Am. Ceram. Soc. 90 (2007) 1965–1988.
[56] R.S. Gates, M. Hsu, E.E. Klaus, Tribochemical mechanism of alumina with water, Tribol. Trans. 32 (1989) 357–363.
[57] Y. Wang, Y. Yang, Y. Zhao, W. Tian, H. Bian, J. He, Sliding wear behaviors of in situ alumina/aluminum titanate ceramic composites, Wear 266 (2009) 1051–1057.
[58] C. Ulrich, H. Petersson, H. Sundgren, F. Björefors, C. Krantz-Rülcker, Simultaneous estimation of soot and diesel contamination in engine oil using electrochemical impedance spectroscopy, Sensor. Actuator. B Chem. 127 (2007) 613–618.
[59] M.P. Brady, G. Rother, L.M. Anovitz, K.C. Littrell, K.A. Unocic, H.H. Elsentriecy, G. L. Song, J.K. Thomson, N.C. Gallego, B. Davis, Film breakdown and nano-porous Mg(OH)2 formation from corrosion of magnesium alloys in salt solutions, J. Electrochem. Soc. 162 (2015) C140–C149.
[60] G. Williams, H. Neil McMurray, Localized corrosion of magnesium in chloride-containing electrolyte studied by a scanning vibrating electrode technique, J. Electrochem. Soc. 155 (2008) C340–C349.
[61] R.E. McNulty, J.D. Hanawalt, Some corrosion characteristics of high purity magnesium alloys, Transactions of The Electrochemical Society 81 (1942) 423–433.
[62] A. Singh, S.P. Harimkar, Laser surface engineering of magnesium alloys: A review, JOM - Journal of the Minerals, Metals and Materials Society 64 (2012) 716–733.
[63] S. Bargir, S. Dunn, B. Jefferson, J. Macadam, S. Parsons, The use of contact angle measurements to estimate the adhesion propensity of calcium carbonate to solid substrates in water, Appl. Surf. Sci. 255 (2009) 4873–4879.
[64] R.N. Wenzel, Resistance of solid surfaces to wetting by water, Ind. Eng. Chem. 28 (1936) 988–994.
[65] R.N. Wenzel, Surface roughness and contact angle, J. Phys. Colloid Chem. 53 (1949) 1466–1467.